THE ASTROPHYSICAL JOURNAL, 565:800–807, 2002 February 1
© 2002. The American Astronomical Society. All rights reserved. Printed in U.S.A.

FAR ULTRAVIOLET SPECTROSCOPIC EXPLORER OBSERVATIONS OF THE SEYFERT 1.5 GALAXY NGC 5548 IN A LOW STATE

M. S. BROTHERTON,[1] R. F. GREEN,[1] G. A. KRISS,[2,3] W. OEGERLE,[4] M. E. KAISER,[3] W. ZHENG,[3] AND J. B. HUTCHINGS[5]

Received 2001 August 3; accepted 2001 September 26

ABSTRACT

We present far-ultraviolet spectra of the Seyfert 1.5 galaxy NGC 5548 obtained in 2000 June with the *Far Ultraviolet Spectroscopic Explorer* (*FUSE*). Our data span the observed wavelength range 915–1185 Å at a resolution of $\sim$20 km s^{-1}. The spectrum shows a weak continuum and emission from O VI $\lambda\lambda$1032, 1038, C III λ977, and He II λ1085. The *FUSE* data were obtained when the active galactic nucleus was in a low state, which has revealed strong, narrow O VI emission lines. We also resolve intrinsic, associated absorption lines of O VI and the Lyman series. Several distinct kinematic components are present, spanning a velocity range of $\sim$0 to $-$1300 km s^{-1} relative to the systemic velocity, with kinematic structure similar to that seen in previous observations of longer wavelength ultraviolet (UV) lines. We explore the relationships between the far-UV absorbers and those seen previously in the UV and X-rays. We find that the high-velocity UV absorption component is consistent with being low ionization, contrary to some previous claims, and is consistent with its nondetection in high-resolution X-ray spectra. The intermediate-velocity absorbers, at $-$300 to $-$400 km s^{-1}, show H I and O VI column densities consistent with having contributions from both a high-ionization X-ray absorber and a low-ionization UV absorber. No single far-UV–absorbing component can be solely identified with the X-ray absorber.

Subject headings: galaxies: active — galaxies: individual (NGC 5548) — galaxies: nuclei — galaxies: Seyfert — quasars: absorption lines — ultraviolet: galaxies — X-rays: galaxies

On-line material: color figures

1. INTRODUCTION

NGC 5548 is among the most studied of Seyfert galaxies. As a bright, nearby ($z = 0.017175$) variable active galactic nucleus (AGN), NGC 5548 in particular has been the target of intensive monitoring campaigns in the optical (e.g., Peterson et al. 1999), the ultraviolet (Clavel et al. 1991; Korista et al. 1995), and the extreme-ultraviolet (Marshall et al. 1997). The time-delayed response of emission lines to continuum changes indicates the size scale of the emitting regions. In the case of NGC 5548, the Doppler widths of the lines and their respective size scales are consistent with Keplerian motion around a black hole of mass $5.9 \times 10^7\ M_\odot$ (Peterson & Wandel 2000).

NGC 5548 is also noteworthy as an AGN with intrinsic ultraviolet (UV) and X-ray absorption characteristic of a high-velocity outflow. About half of all Seyfert galaxies display complex narrow intrinsic absorption of high-ionization species with transitions in the UV (Crenshaw et al. 1999). Moreover, there appears to be a one-to-one correspondence between the presence of this UV absorption and warm X-ray absorption. Warm absorbers appear to be highly ionized (typically $U = 0.1$–10, where U is the ratio of the number density of hydrogen-ionizing photons to the hydrogen number density) with total column densities in the range 10^{21}–10^{23} cm^{-2} (George et al. 1998).

The correspondence between the presence of UV absorption and X-ray absorption suggests a direct link between the two despite the ionization difference. Mathur, Elvis, & Wilkes (1995) proposed a single-zone model for a combined UV–X-ray absorber in NGC 5548. High-resolution UV spectroscopy shows that the UV absorber is resolved into distinct kinematic components with outflow velocities ranging to more than 1100 km s^{-1} (Mathur, Elvis, & Wilkes 1999; Crenshaw & Kraemer 1999) and with a range of ionization states and column densities.

The new generation of X-ray telescopes (*Chandra*, *XMM*) now provide the combination of sensitivity and spectral resolution to detect and measure the kinematic properties of X-ray absorption lines in AGNs. Kaastra et al. (2000) presented the first high-resolution X-ray spectrum of a Seyfert galaxy, in fact, NGC 5548. The *Chandra* Low Energy Transmission Grating Spectrograph (LETGS) spectrum revealed strong narrow absorption lines from highly ionized species, blueshifted by several hundred km s^{-1}.

The *Far Ultraviolet Spectroscopic Explorer* (*FUSE*) (Moos et al. 2000) provides spectral coverage of shorter wavelengths than possible with the *Hubble Space Telescope* (*HST*). Of special interest in this wavelength range for investigations of the intrinsic UV–X-ray absorbers is the O VI $\lambda\lambda$1032, 1038 resonance doublet, as O VI is of intermediate ionization. In the warm absorber in Mrk 509, for instance, *FUSE* resolves seven kinematic components of intrinsic O IV absorption, one of which—and only one of which—can be identified with the X-ray absorber (Kriss et al. 2000). Kriss (2000) reviewed this result along with other *FUSE* observations of AGNs.

[1] Kitt Peak National Observatory, National Optical Astronomy Observatories, P.O. Box 26732, 950 North Cherry Avenue, Tucson, AZ 85726-6732; mbrother@noao.edu, green@noao.edu.

[2] Space Telescope Science Institute, 3700 San Martin Drive, Baltimore, MD 21218.

[3] Center for Astrophysical Sciences, Department of Physics and Astronomy, The Johns Hopkins University, Baltimore, MD 21218-2686.

[4] Laboratory for Astronomy and Solar Physics, NASA Goddard Space Flight Center, Code 681, Greenbelt, MD 20771.

[5] Herzberg Institute of Astrophysics, National Research Council of Canada, Victoria, BC V9E 2E7, Canada; john.hutchings@hia.nrc.ca.

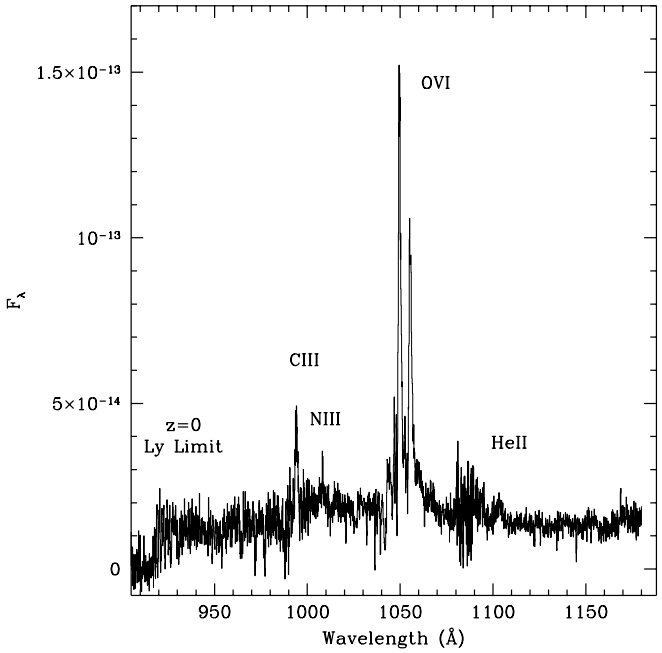


FIG. 1.—Full-range display spectrum with 0.1 Å bins; this is a coarser binning than that used for analysis and is used here for display only. Geocoronal emission lines have been removed. Prominent features are labeled. The flux units are ergs s^{-1} cm^{-2} $Å^{-1}$. The low signal-to-noise ratio for 1080–1100 Å results from the fact that only a single SiC channel contributes at those wavelengths.

In this paper we present *FUSE* observations of NGC 5548 (§ 2), focusing in particular on characterizing the intrinsic O VI and Lyβ absorption components (§ 3). We interpret the spectral features with the assistance of photoionization models (§ 4) and discuss our findings together with the previous results from the UV and X-ray to achieve an improved understanding of the ionized outflow of NGC 5548 (§ 5).

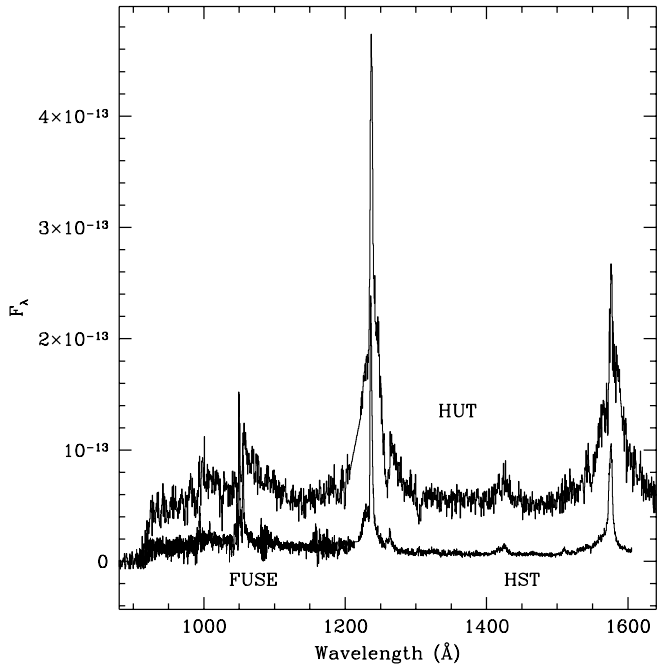


FIG. 2.—Comparison between the (2000) *FUSE* spectrum, a previous epoch (1991) low-state Faint Object Spectrograph (FOS) spectrum from *HST* (Crenshaw et al. 1993), and a Hopkins Ultraviolet Telescope (HUT) spectrum of NGC 5548 in the high state (Kriss et al. 1997).

2. OBSERVATIONS

FUSE (Moos et al. 2000; Sahnow et al. 2000) contains four "channels" that are in effect four independent telescope/grating spectrographs, two of which employ optics coated with LiF for high efficiency from ~990 to 1187 Å and two of which employ optics coated with SiC for high efficiency at shorter wavelengths. Two two-dimensional photon-counting microchannel plate detectors record spectra from the four channels.

NGC 5548 was observed on 2000 June 7 through the 30″ × 30″ low-resolution aperture with a total exposure time of 25 ks. Data were recorded in photon-address mode, which provides a time-tagged list of event positions in the downlinked data stream. All channels were aligned, resulting in spectra covering the whole wavelength range from 905 to 1187 Å.

To calibrate the data, we use a modified version of the standard *FUSE* pipeline. Our processing restricts the pulse heights for acceptable data to channels 4–16 to reduce the background. We also scale the background level to match the levels seen in blank regions of the detector. Because *FUSE* uses the LiF1 channel for fine guidance, this channel has the best photometric accuracy and the best absolute wavelength scale. We therefore cross-correlate the other three channels with LiF1 to obtain adjustments to the zero points of their wavelength scales, and we scale their fluxes to match the level seen in LiF1. To obtain the best signal-to-noise ratio (S/N) in our final calibrated spectrum, we rebin the data from all the detector segments onto a uniform wavelength scale using 0.05 Å bins. Approximately 7 pixels from each detector segment contribute to each bin. This results in an effective spectral resolution of ~20 km s^{-1}. We estimate that our fluxes are accurate to ~10% and that the wavelength scale has an absolute accuracy of ~15 km s^{-1}.

Figure 1 displays the full *FUSE* spectrum. We note the presence of emission lines of O VI $\lambda\lambda$1032, 1038, C III λ977, N III λ990, and He II λ1085. We do not see an intrinsic Lyman edge. Galactic molecular hydrogen appears present but weak along this sight line, and a number of atomic lines from the Galactic ISM are present as well (including O VI $\lambda\lambda$1032, 1038). A Galactic Lyman edge is also seen.

NGC 5548 was in a low state when observed by *FUSE*. Coincidently, this low state appears to match the flux level of NGC 5548 in 1991 when first observed with the Faint Object Spectrograph (FOS) on *HST* (Crenshaw, Bogges, & Wu 1993). This level is a factor of several lower than when observed in recent years by, for instance, the Hopkins Ultraviolet Telescope (HUT; Kriss et al. 1997). Figure 2 compares these spectra. In the low state the continuum and broad lines weaken and the less time-variable narrow lines become more prominent.

3. SPECTRAL MEASUREMENTS

Given the low state of NGC 5548, the S/N of the spectrum is not as high as initially anticipated. For $\lambda < 1000$ Å the S/N per 0.05 Å pixel is only about 3; we therefore cannot make accurate measurements of C III λ977 and the higher order Lyman lines, although some degree of absorp-

tion is probably present (contaminating Galactic O I λ989 certainly is present). At longer wavelengths in the Lyβ and O VI region, the S/N is about 10 in the continuum and higher in the emission lines. This is large enough for detailed work at the full resolution of *FUSE*.

We make measurements of the Lyβ/O VI region using our 0.05 Å combined-channel spectrum. We use SPECFIT (Kriss 1994) to fit the spectral region. The continuum is modeled as a power law plus Galactic extinction (A_B = 0.088 mag; Schlegel, Finkbeiner, & Davis 1998) using the reddening curve of Cardelli, Clayton, & Mathis (1989) with $R_V = 3.1$. The O VI emission lines are fitted using Gaussian components. Since inflections are present in the emission profiles, these separate components may have physical significance. O VI $\lambda\lambda$1032, 1038 is a doublet with an optically thin line ratio of 2:1, but in dense gas with saturation the ratio may approach 1:1. While the physical conditions typically associated with the narrow-line region (NLR) should show only the 2:1 O VI $\lambda\lambda$1032, 1038 doublet emission ratio, the ratio is 1:1 in the low-state *FUSE* spectrum of NGC 3516 (Hutchings et al. 2001). Given this empirical result and the possibility of narrow O VI $\lambda\lambda$1032, 1038 emitting gas with atypical conditions, our initial models begin with 2:1 doublet ratios but are allowed to vary between 2:1 and 1:1.

We approximate the intrinsic absorption as several components with Gaussian distributions in optical depth that are permitted to partially cover the background source. The optical depth ratio of the doublets is constrained to be 2:1 at all velocities. The initial parameters for the Gaussians (e.g., FWHM, redshift) are selected to match those reported for UV lines (components 1–6) by Crenshaw & Kraemer (1999) but allowed to freely vary to account for source variability, ionization differences, and data quality. We also add two new components, a high-velocity component "0.5" and a component "2.5," which significantly improved the fits. The absorption lines of the O VI doublets and Lyβ are fitted simultaneously and constrained to have the same covering fraction.[6]

Column densities for a particular ionized species are obtained from measurements of optical depth according to the equation

$$N_{\rm ion} = \frac{3.7679 \times 10^{14}\ {\rm cm}^{-2}}{\lambda f} \int \tau(v) dv\ {\rm km\ s}^{-1}\ , \qquad (1)$$

where λ is the transition wavelength and f is the pertinent oscillator strength. The units on columns discussed below will always be cm^{-2}, which will be implicitly understood for the case of logarithmic columns. For O VI λ1032, log $\lambda f = 2.137$, and for Lyβ, log $\lambda f = 1.909$ (Morton 1991), where λ is in Å. For the case of absorption lines that have Gaussians in optical depth,

$$\int \tau(v) dv = 1.0645 \times {\rm FWHM} \times \tau_0\ , \qquad (2)$$

where τ_0 is the optical depth at zero velocity and the FWHM is in km s^{-1}.

[6] The partial covering of absorption components in principle can vary between red and blue doublets since the ratios of different emission components with potentially different individual coverings can differ. In instances like this one, permitting this extra freedom in the fitting, however, compromises the consistency of the results.

Contaminating Galactic lines are included in the models. We note in particular that O I λ1039 and Ar I λ1048 fall at the same wavelengths as redshifted intrinsic absorption troughs (Ar I λ1048 is constrained by simultaneously fitting Ar I λ1066). The atomic transitions are constrained to have the same line widths. Several strong Galactic molecular hydrogen lines absorb some of the blue peak of O VI emission.

3.1. *Specific Models*

There are two primary classes of models that yield plausible fits to the spectrum. The first class, and the one we favor, features narrow emission lines with FWHM $\sim$400 km s^{-1} that are uncovered by absorption components. These emission lines may be associated with a traditional extended low-density NLR. A small degree of skewness in the form of a blue tail is allowed by the model and consistent with NLR profiles (e.g., Brotherton 1996). The weak broad emission is fit using the sum of two Gaussians. These emission lines are described in Table 1 and shown as green dotted lines in Figure 3. The redshift of the narrow emission lines in this case is 0.01702, only 50 km s^{-1} blueshifted from the 21 cm redshift of $z = 0.017175$, and clearly larger than the "emission-line redshift" of $z = 0.01676$ given in the NASA/IPAC Extragalactic Database (NED). Table 2 gives the parameters for the absorption components in our best-fitting model.

The second class of models involves a significant extrapolation of the narrow emission components, in which we assume that the NLR is at least partially covered by the absorbers. The motivations for this type of model are that the high-ionization NLR is expected to be compact

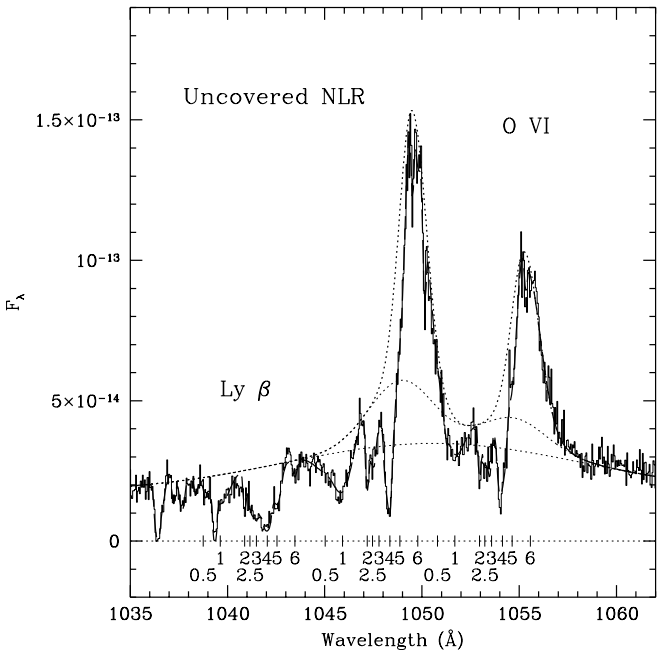


FIG. 3.—Our preferred SPECFIT model (*heavy dashed line*) of the combined-channel spectrum (0.5 Å bins) of O VI $\lambda\lambda$1032, 1038 and Lyβ. The model has $\chi^2 = 1240.2$ for 801 points and 85 degrees of freedom. The light dotted line indicates emission components. The absorption lines were assumed to at least partially cover the broad lines and continuum but not the narrow emission-line component. The dotted line indicates zero flux. The central wavelengths of the absorbing components in Table 2 are marked. [*See the electronic edition of the Journal for a color version of this figure.*]

TABLE 1

MODEL O VI EMISSION-LINE PARAMETERS

Feature	Observed λ (Å)	Flux[a] (10^{13} ergs s^{-1}cm^{-2})	FHWM (km s^{-1})	Velocity[b] (km s^{-1})
Uncovered NLR Model				
Broad O VI λ1032	1048.94	2.29 ± 0.04	4841 ± 89	−200
Broad O VI λ1038	1054.72	1.14	4841	−200
Intermediate O VI λ1032.....	1048.94	0.95 ± 0.04	1111 ± 47	−200
Intermediate O VI λ1038.....	1054.72	0.47	1111	−200
Narrow O VI λ1032	1049.49 ± 0.04	1.69 ± 0.10	432 ± 12	−50
Narrow O VI λ1038	1055.26	1.06 ± 0.03	432	−50
Covered NLR Model				
Broad O VI λ1032	1048.94 ± 0.05	2.34 ± 0.05	4366 ± 107	−200
Broad O VI λ1038	1054.7	1.17	4366	−200
Narrow O VI λ1032	1049.32 ± 0.05	3.27 ± 0.03	658 ± 9	−90
Narrow O VI λ1038	1054.11	1.65 ± 0.03	658	−90

NOTE.—Values without uncertainties are either tied to another parameter or became fixed during the fitting process.

[a] These are observed fluxes. If the Galactic reddening is assumed to be $E(B-V) = 0.02$ mag for the extinction of Cardelli et al. 1989, then these fluxes should be increased by 30%.

[b] Velocities are relative to systemic $z = 0.017175$ (H I 21 cm, NED).

(Kraemer et al. 1998) and hence more easily covered, that the narrow-line component of the UV lines seen in the low-state FOS spectrum has a FWHM $\sim$ 1000 km s^{-1} (Goad & Koratkar 1998), and that low-state narrow O VI emission appears to arise at small radii at the base of an accelerating wind in NGC 3516 (Hutchings et al. 2001). Our best covered NLR model has a narrow emission component with a FWHM $\sim$ 650 km s^{-1}, larger than that of the uncovered case and more similar to the Goad & Koratkar (1998) results. Figure 4 shows this model, and Tables 1 and 2 give the model parameters. Table 1 reveals that the narrow O VI doublet ratio is an optically thin 2:1, unlike the case of NGC 3516 where it is nearly 1:1 (Hutchings et al. 2001), weakening the similarity between the two AGNs in the low state.

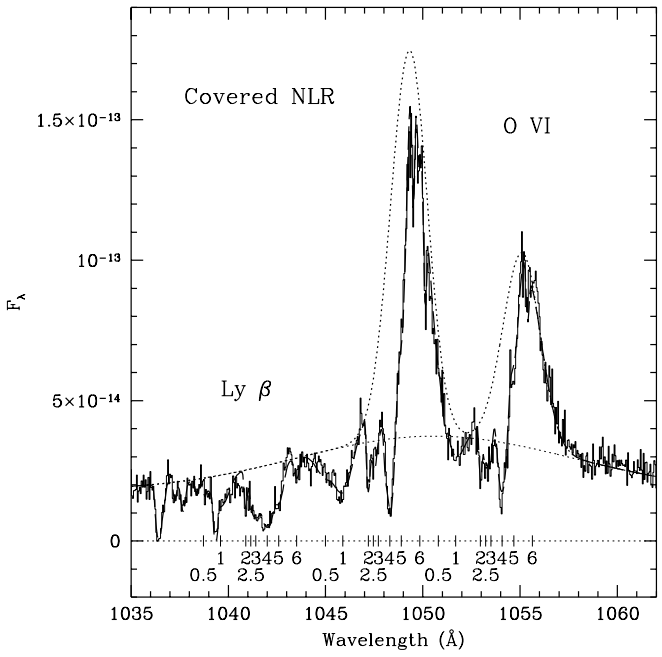


FIG. 4.—An alternative SPECFIT model (*heavy dashed line*) of the combined-channel spectrum (0.5 Å bins) of O VI $\lambda\lambda$1032, 1038 and Lyβ. The model has $\chi^2 = 1356.4$ for 801 points and 82 degrees of freedom. The light dotted line indicates emission components. In this case the absorption lines were assumed to at least partially cover all emission components. The dotted line indicates zero flux. The central wavelengths of the absorbing components in Table 2 are marked. [*See the electronic edition of the Journal for a color version of this figure.*]

While we favor the uncovered NLR model as it is less of an extrapolation and yields a better χ^2, an examination of Table 2 reveals that both models give very similar results for the absorption lines. Despite the possible uncertainty about the FWHM and covering of the narrow emission lines, the inferred absorption-line column densities and ratios appear rather robust.

3.2. *Continuum*

We also make independent fits to measure the continuum slope, expanding the fitting range beyond the immediate vicinity of O VI and Lyβ and excluding portions of spectra with clear emission or absorption present. Assuming only a power-law continuum shape and Galactic reddening, the power-law index obtained is $\alpha = -1.23 \pm 0.11$, where $F_\nu \propto \nu^\alpha$.

4. INTRINSIC ABSORPTION IN NGC 5548

We interpret the absorbing column densities in Table 2 with the assistance of photoionization models. We have employed the latest version of CLOUDY (C94; Ferland 2001). We assume solar abundances and the continuum shape of Dumont, Collin-Souffrin, & Nazarova (1998). We characterize the state of the gas in terms of the dimensionless ionization parameter U, which is the ratio of the number density of hydrogen-ionizing photons to the number density of hydrogen. Within our *FUSE* spectrum we can measure simultaneous column densities for only neutral hydrogen and O VI. The physical conditions of an absorber are not uniquely determined with only H I and O VI column densities. In general there will be two solutions, one with a low ionization parameter and low total column density and another with a high ionization parameter and higher column density. For gas in both very low

TABLE 2

MODEL ABSORPTION PARAMETERS

Feature	Observed λ (Å)	Column Density (10^{12} cm^{-2})	FWHM (km s^{-1})	Covering Fraction[a]	Velocity[b] (km s^{-1})
Uncovered NLR Model: O VI λ1032					
0.5.....	1045.03 ± 0.11	229 ± 33	347 ± 154	1.00	−1320
1.....	1045.92 ± 0.03	544 ± 29	278 ± 17	0.99 ± 0.10	−1070
2.....	1047.19 ± 0.01	296 ± 57	43 ± 17	0.66 ± 0.05	−700
2.5.....	1047.46 ± 0.02	680 ± 154	62 ± 11	0.41 ± 0.10	−630
3.....	1047.79 ± 0.02	208 ± 28	142 ± 12	0.75 ± 0.06	−530
4.....	1048.35 ± 0.01	2121 ± 242	101 ± 4	0.89 ± 0.02	−370
5.....	1048.86 ± 0.04	793 ± 68	125 ± 10	0.94 ± 0.08	−230
6.....	1049.78 ± 0.05	25 ± 18	69 ± 5	1.00	+40
Uncovered NLR Model: Lyβ					
0.5.....	1038.75	87 ± 75	347	1.00	−1320
1.....	1039.63	777 ± 123	278	0.99	−1070
2.....	1040.89	340 ± 302	43	0.66	−700
2.5.....	1041.16	256 ± 50	62	0.41	−630
3.....	1041.49	1830 ± 1406	142	0.75	−530
4.....	1042.04	1589 ± 600	101	0.89	−370
5.....	1042.55	498 ± 225	125	0.94	−230
6.....	1043.47	77 ± 32	69	1.00	+40
Covered NLR Model: O VI λ1032					
0.5.....	1045.00 ± 0.08	282 ± 31	289 ± 35	0.99 ± 0.12	−1330
1.....	1045.89 ± 0.06	473 ± 104	253 ± 34	0.98 ± 0.06	−1080
2.....	1047.20 ± 0.01	315 ± 45	41 ± 12	0.67 ± 0.16	−700
2.5.....	1047.45 ± 0.02	688 ± 139	60 ± 10	0.47 ± 0.04	−630
3.....	1047.72 ± 0.01	313 ± 38	99 ± 6	0.72 ± 0.03	−550
4.....	1048.30 ± 0.03	1692 ± 188	129 ± 7	0.85 ± 0.08	−390
5.....	1048.90 ± 0.01	369 ± 21	143 ± 6	0.94 ± 0.14	−210
6.....	1049.84 ± 0.11	1.1 ± 1.0	78 ± 36	1.00	+50
Covered NLR Model: Lyβ					
0.5.....	1038.72	125 ± 220	289	0.99	−1330
1.....	1039.60	816 ± 262	253	0.98	−1080
2.....	1040.90	325 ± 102	41	0.67	−700
2.5.....	1041.16	256 ± 203	60	0.47	−630
3.....	1041.42	1346 ± 575	99	0.72	−550
4.....	1042.00	2039 ± 330	129	0.85	−390
5.....	1042.59	560 ± 145	143	0.94	−210
6.....	1043.52	109 ± 31	78	1.00	+50

NOTE.—Values without uncertainties either are tied to another parameter (e.g., the Lyβ wavelengths) or became fixed during the fitting process because of imposed limits.

[a] The covering fraction of the absorbing components is with respect to all emission components except the narrow emission lines for the case of the "uncovered" model.

[b] Velocities given are the component Gaussian central wavelengths relative to systemic $z = 0.017175$ (H I 21 cm, NED).

and very high ionization states, there is no O VI as all the oxygen is in lower or higher ionization states, respectively. As a function of increasing ionization parameter, the ratio of H I to O VI column densities starts at zero, rises and peaks ($\sim$10 near log $U \sim 0$ for our models), then falls again. The CLOUDY command *optimize* is used to find solutions without creating large grids in parameter space. Table 3 gives both solutions for the column densities measured for each component in our preferred uncovered NLR fit.

Although the formal errors on many component parameters are small, there is a certain degree of arbitrariness in the models resulting from the blending of the fitted components (especially in conjunction with partial covering). With the addition of two components and freely varying velocity widths, and possible variability, a component-to-component comparison with UV absorbers seen by *HST* (e.g., Crenshaw & Kraemer 1999; Mathur et al. 1999) remains imperfect. Figure 5 shows the velocities of the six *HST* components on a blowup of the blue O VI doublet; it appears that the *FUSE* spectrum is redshifted some 100 km s^{-1} relative to the Space Telescope Imaging Spectrograph (STIS) spectrum. An examination of Galactic lines in the STIS spectrum using on-the-fly calibration suggests that 50 km s^{-1} of the shift may arise there. Potential variability and low spectral resolution in the X-rays also limit comparison with *Chandra* spectra (Kaastra et al. 2000). Still, there is much to be learned from such comparisons assisted by our photoionization models. We do so below.

TABLE 3

PHOTOIONIZATION MODELS

		LOW		HIGH	
COMPONENT	$N_{O\,VI}/N_{H\,I}$	log U	log N_H (cm^{-2})	log U	log N_H (cm^{-2})
0.5	2.63	−1.28	18.0	−0.16	19.5
1	0.70	−1.71	18.4	0.26	21.1
2	0.87	−1.66	18.1	0.20	20.7
2.5	2.66	−1.28	18.4	−0.15	20.0
3	0.11	−2.05	18.4	0.56	22.0
4	1.33	−1.55	18.9	0.11	21.2
5	1.59	−1.48	18.5	0.03	20.6
6	0.32	−1.88	17.3	0.42	20.4

NOTE.—Input column densities are for the uncovered NLR model fit. Given only $N_{O\,VI}$ and $N_{H\,I}$ column densities, both a high (U, N_H) and low (U, N_H) solution can be found using CLOUDY.

4.1. *Components 0.5 and 1*

We first consider high-velocity components (−1000 to −1300 km s^{-1}). The blue O VI absorption at these velocities is beyond any uncertainties in the O VI narrow emission lines. Component 1 is also of special interest because Crenshaw & Kraemer (1999) claim, based on the column density ratio of N(N V)/N(C IV) seen in GHRS *HST* spectra, that this component has a high ionization parameter and large column density and could be a manifestation of the X-ray absorber.

Crenshaw & Kraemer (1999) started with N(N V)/N(C IV) = 18 ± 7, based on nonsimultaneous GHRS spectra taken 6 months apart of the N V and C IV spectral regions. Their preferred physical conditions for a model to account for this single column density ratio were

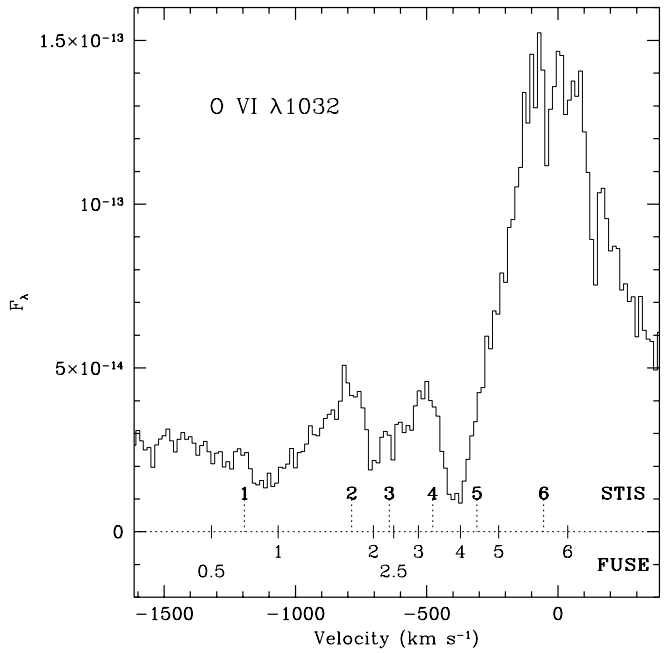


FIG. 5.—Blowup of the blue doublet of O VI on a velocity scale (assuming $z = 0.017175$). Numbers/tick marks below zero show the positions of the fitting components just as in the uncovered NLR model of Fig. 3. Numbers/tick marks above zero indicate the velocities of Crenshaw & Kraemer's (1999) components 1–6 based on the *HST* STIS spectrum. It would appear that there is a velocity shift of ∼100 km s^{-1} or less between the two, probably the result of calibration uncertainties.

log $U = 0.38$ and effective hydrogen column density of log $N_H = 21.8$. They investigated varying U or N_H in order to explain their later epoch STIS spectrum, for which N(N V) was lower, N(H I) was known, and N(C IV) had an upper limit. These resulted in similarly high U, high N_H conditions for the component 1 absorber.

Table 3 shows our pair of solutions for component 1 (ignoring the weaker and more uncertain component 0.5): (1) log $U = 0.26$, total hydrogen column log $N_H = 21.1$; (2) log $U = -1.71$, total hydrogen column log $N_H = 18.4$. From Crenshaw & Kraemer (1999), we might be led to assume our high-ionization solution represents the conditions in component 1. The *HST* spectra were taken when NGC 5548 was in a high state (within a few percent of the level of the HUT spectrum in Fig. 2), so we might expect a somewhat lower ionization parameter in the low-state *FUSE* spectrum, just as we see.

We find using the N(N V)/N(C IV) GHRS spectra ratio alone suspect: first, the two spectral regions were observed six months apart (Crenshaw et al. 1999) and absorbers have been seen to vary on this timescale; second, N V and C IV have similar ionization states and the column density ratio is rather insensitive to the ionization parameter (small uncertainties in the ratio correspond to large differences in U); and third, nitrogen abundances have been found to be preferentially enhanced in AGN (primarily in high-luminosity AGNs, e.g., Hamann & Ferland 1993), and to have significant scatter—assuming solar abundances is a large source of uncertainty. The GHRS N(N V)/N(C IV) constraint would seem to be a poor one. We elect to make our own comparison for the STIS spectrum alone, which has simultaneous measurements (or interesting upper limits) for three species.

In order to make a consistent comparison, we use CLOUDY with the Dumont et al. (1998) spectral energy distribution to model the physical conditions of the absorber using the column densities reported by Crenshaw & Kraemer (1999) for the STIS spectrum (in the case of C IV λ1549 only an upper limit is available). We find a good *low*-ionization solution, with log $U = -0.94$ and a total column density of log $N_H = 18.7$. Using instead the Crenshaw & Kraemer (1999) continuum changes the solution to log $U = -0.38$ and log $N_H = 19.3$—higher ionization and larger column density but still far from their high-ionization values.

These low-ionization solutions are not dissimilar to our low-ionization solution for the *FUSE* spectrum. In fact, the ionization parameter (log $U = -1.7$) appears lower for the low-state spectrum as we might expect. Is there a way to decide whether the "low" or "high" solution is correct?

The *Chandra* spectrum of Kaastra et al. (2000) shows no O VII and O VIII absorption at the velocity of component 1, while the "high" solution would predict easily detectable columns on order of log $N \sim 17$–18. The *Chandra* spectrum does show O VI absorption at component 1 velocities, entirely consistent with the *FUSE* "low" solution and our solution for the STIS column densities. We conclude that component 1 is a low column density, low-ionization absorber with the properties described above.

4.2. *Components 2–5*

Components 2–5 correspond to absorption between velocities of −700 and −200 km s^{-1}. This complex is of special interest because strong absorption is seen in both

longer wavelength UV lines and in higher ionization X-ray transitions.

The absorption structure is very similar to that seen in the UV lines like C IV λ1549 (Crenshaw & Kraemer 1999; Mathur et al. 1999). Different fitted components, blending, and variability issues conspire to make a one-to-one component comparison between the *FUSE* and *HST* spectra difficult, but the general findings are of interest. Crenshaw & Kraemer (1999) find ionization parameters of a few tenths and total hydrogen columns of 10^{19}–10^{20} cm^{-2}. These conditions produce O VI columns on the order of 10^{15} cm^{-2} and are consistent with our "low" models of Table 3.

But what of the X-ray absorption? Kaastra et al. (2000) found significant column densities for a number of high-ionization species [e.g., log N(O VII) = 17.2 and log N(O VIII) = 18.1]. The X-ray absorption appears centered at a velocity of -400 km s^{-1} (using $z = 0.017175$) and has a FWHM $\sim$ 600 km s^{-1}; Kaastra et al. suggested that the large span in velocity is suggestive of contributions of several individual components of smaller velocity dispersion. We put the column densities reported by Kaastra et al. into CLOUDY with the Dumont et al. (1998) continuum and find a good solution similar to that of Kaastra et al.: log $U = 0.43$ and log $N_{\rm H} = 21.8$. This model predicts log N(O VI) = 14.8 and log N(H I) = 15.3, less than what we observe from the sum of the components in the *FUSE* spectrum but enough to account for an individual component or two. Such conditions predict very low column densities for C IV and N V. This may in part explain why we needed to add a component "2.5," although variability could also be involved.

Based on CLOUDY models, an O VI column density on the order of log N(O VI) = 15 would appear to be consistent with *both* the X-ray and UV absorbers. We cannot unambiguously say if any individual O VI absorbing component arises solely from high-ionization or low-ionization gas. Simultaneous high-resolution UV/far-UV/X-ray spectra would help unravel the physical conditions of the outflowing material along the line of sight.

4.3. *Component 6*

Component 6 poses a special problem. The velocity of this component falls at the apparent peak of the O VI emission, where the covering is most uncertain and contaminating molecular H_2 lines are present. The formal fitting uncertainties in Table 2 indicate that we do not reliably measure O VI or Lyβ absorption in component 6. Crenshaw & Kraemer (1999) summarily dismissed this component as uninteresting given that it was at low velocity and appeared only in Lyα and not in C IV λ1549 or N V λ1240.

5. DISCUSSION

Intrinsic absorption is seen in the *FUSE* spectrum of NGC 5548 in the low state in hydrogen Lyβ and in O VI $\lambda\lambda$1032, 1038. The velocity range and kinematic structure closely resembles that seen previously by high-resolution *HST* spectra in the UV (Mathur et al. 1999; Crenshaw & Kraemer 1999). At least some portion of the O VI–absorbing gas would seem to be identifiable with the previously studied UV absorber, variability notwithstanding.

Reanalysis of the STIS data, in conjunction with our *FUSE* spectrum, indicates that the high-velocity component 1 is *not* high ionization and is not the X-ray warm absorber. This reconciles the results of Kaastra et al. (2000), who reported that high-ionization species have a blueshift of 280 $\pm$ 70 km s^{-1} (for $z = 0.01676$; using $z = 0.017175$ increases the blueshift by 120 km s^{-1} to $\sim$400 km s^{-1}, consistent with component 3 or 4). Mathur et al. (1999) suggested that the broad component 3 ($\sim$300 km s^{-1} FWHM) could be identified with the X-ray absorber. The blueshift of the X-ray absorber and component 3 would tend to support this conclusion, although there may simply exist material along the line of sight with a range of physical conditions at these velocities. High-resolution, high S/N, simultaneous spectra of the UV, far-UV, and X-ray regions are required to finally determine the nature of the absorbing components along the line of sight.

Despite the one-to-one correspondence between the incidence of X-ray absorption and UV absorption in the 50%–60% of Seyfert galaxies that show such absorption, there is not one-to-one correspondence at the level of individual kinematic components. These outflows are clearly stratified in some fashion. The UV absorbers often appear as distinct components at a range of velocities, appearing and vanishing over the timescales of months to years (some of course are more stable). In Mrk 509 there are seven components, only one of which appears to be high ionization, and it is near zero velocity (Kriss et al. 2000). In NGC 3783 the X-ray absorber is blueshifted by 610 km s^{-1} (Kaspi et al. 2001); the resolution at X-ray wavelengths is not yet sufficient to separate any kinematic components. Still, we may conclude that there is no simple relationship between ionization and velocity, and as yet no clear hint about their dynamical or physical structure (although radiative acceleration appears likely in a number of cases including NGC 5548; Srianand 2000).

Thermally driven wind models such as those proposed by Krolik & Kriss (1995, 2001) also are consistent with the observations. These winds are evaporated from the surface of the obscuring torus and they have low velocities compatible with those typically seen in Seyfert 1 galaxies. At the critical ionization parameter for evaporation in these models, there is a broad range of temperatures that can coexist in equilibrium at nearly constant pressure. Thus the flow is expected to be strongly inhomogeneous. High-temperature, highly ionized gas causing X-ray absorption can coexist with more densely clumped, lower temperature gas that forms UV absorption lines.

The nature of the narrow emission lines has been only a minor complication for studying the intrinsic absorption in far-UV, by coincidence as much as anything else. For a high-state spectrum, such as those obtained by *HST*, deducing if uncovered narrow emission lines fill in deep trough bottoms can have a profound effect on measured columns (e.g., Arav, Korista, & de Kool 2002). The narrow O VI emission lines are of special interest in their own right. How narrow are they? Are they covered?

The narrow-line region of NGC 5548 is extended, with deep narrowband images showing [O III] λ5007 spanning a region some 4×2.7 kpc^2 aligned with the weak radio structure (Wilson et al. 1989). Moore, Cohen, & Marcy (1996), using optical spectra, found that the line widths and line shifts of narrow emission lines correlated with the critical density of the transition rather than ionization potential and that the low critical density lines are in fact consistent with the 21 cm redshift of 0.017175. The FWHM of these optical narrow lines ranges from 300 to 500 km s^{-1}. This is entirely consistent with what we find for our preferred

uncovered NLR model, and so perhaps we should not be concerned that Goad & Koratkar (1998) found for the low-state FOS spectrum (Crenshaw et al. 1993) FWHMs on the order of 1000 km s^{-1} for UV narrow lines like C IV λ1549. That was a single-epoch low-resolution spectrum. Likewise, the NLR models of Kraemer et al. (1998) suggest that the high-ionization narrow-line region is rather compact (parsec scale) and may easily be covered. Their model, however, underpredicts the observed narrow O VI emission lines by nearly an order of magnitude.

6. SUMMARY

We have presented the far-ultraviolet spectrum of NGC 5548 observed by *FUSE* in a low state. Prominent narrow O VI $\lambda\lambda$1032, 1038 emission lines are present, as are intrinsic absorption lines of O VI and hydrogen Lyβ. Two rather different assumptions regarding the narrow O VI emission lines both lead to rather similar measurements of the absorbing column densities. Reanalysis of the UV column densities of the highest velocity component (1) reported by Crenshaw & Kraemer (1999) indicates a low total column density and low ionization parameter and is consistent with our *FUSE* results and consistent with the lack of an X-ray absorber at this velocity (Kaastra et al. 2000). The absorbers with intermediate velocities of -200 to -700 km s^{-1} are primarily identified with the same low ionization parameter, low column density material that absorbers at longer UV wavelengths, but almost certainly have some non-negligible contribution from the high ionization parameter, high column density material that results in absorption lines seen in the X-ray. Still, no single component of O VI absorption can be unambiguously identified as "the X-ray absorber." High-quality, simultaneous multiwavelength spectra at several epochs may be required to fully understand the emitting and absorbing regions.

We thank Nahum Arav, Qirong Yuan, and Steve Kraemer for useful comments. This work is based on data obtained for the Guaranteed Time Team by the NASA-CNES-CSA *FUSE* mission operated by the Johns Hopkins University. Financial support to U.S. participants has been provided by NASA contract NAS 5-32985. This research has made use of the NASA/IPAC Extragalactic Database (NED), which is operated by the Jet Propulsion Laboratory, California Institute of Technology, under contract with the National Aeronautics and Space Administration.

REFERENCES

Arav, N., Korista, K. T., & de Kool, M. 2002, ApJ, in press
Brotherton, M. S. 1996, ApJS, 102, 1
Cardelli, J. A., Clayton, G. C., & Mathis, J. S. 1989, ApJ, 345, 245
Clavel, J., et al. 1991, ApJ, 366, 64
Crenshaw, D. M., Boggess, A., & Wu, C. 1993, ApJ, 416, L67
Crenshaw, D. M., & Kraemer, S. B. 1999, ApJ, 521, 572
Crenshaw, D. M., Kraemer, S. B., Boggess, A., Maran, S. P., Mushotzky, R. F., & Wu, C. 1999, ApJ, 516, 750
Dumont, A., Collin-Souffrin, S., & Nazarova, L. 1998, A&A, 331, 11
Ferland, G. J. 2001, Hazy, a Brief Introduction to CLOUDY 94.00 (Univ. Kentucky. Dept. Phys. Astron. Int. Rep.)
George, I. M., Turner, T. J., Netzer, H., Nandra, K., Mushotzky, R. F., & Yaqoob, T. 1998, ApJS, 114, 73
Goad, M., & Koratkar, A. 1998, ApJ, 495, 718
Hamann, F., & Ferland, G. 1993, ApJ, 418, 11
Hutchings, J. B., et al. 2001, ApJ, 559, 173
Kaastra, J. S., Mewe, R., Liedahl, D. A., Komossa, S., & Brinkman, A. C. 2000, A&A, 354, L83
Kaspi, S., et al. 2001, ApJ, 554, 216
Korista, K. T., et al. 1995, ApJS, 97, 285
Kraemer, S. B., Crenshaw, D. M., Filippenko, A. V., & Peterson, B. M. 1998, ApJ, 499, 719
Kriss, G. 1994, in ASP Conf. Ser. 61, Astronomical Data Analysis Software and Systems III, ed. D. R. Crabtree, R. J. Hanisch, & J. Barnes (San Francisco: ASP) 437
Kriss, G. A. 2000, First Results from the *FUSE* Mission, 24th meeting of the IAU, Joint Discussion 11, August 2000, Manchester, England., 11, E7
Kriss, G. A., et al. 2000, ApJ, 538, L17
Kriss, G., Krolik, J., Grimes, J., Tsvetanov, Z., Espey, B., Zheng, W., & Davidsen, A. 1997, in IAU Colloq. 159, Emission Lines in Active Galaxies: New Methods and Techniques, ed. B. M. Peterson, F.-Z. Cheng, & A. S. Wilson (ASP Conf. Ser. 113; San Francisco: ASP), 453
Krolik, J. H., & Kriss, G. A. 1995, ApJ, 447, 512
———. 2001, ApJ, 559, 173
Marshall, H. L., et al. 1997, ApJ, 479, 222
Mathur, S., Elvis, M., & Wilkes, B. 1995, ApJ, 452, 230
———. 1999, ApJ, 519, 605
Moore, D., Cohen, R. D., & Marcy, G. W. 1996, ApJ, 470, 280
Moos, H. W., et al. 2000, ApJ, 538, L1
Morton, D. C. 1991, ApJS, 77, 119
Peterson, B. M., et al. 1999, ApJ, 510, 659
Peterson, B. M., & Wandel, A. 1999, ApJ, 521, L95
Sahnow, D. J., et al. 2000, ApJ, 538, L7
Schlegel, D. J., Finkbeiner, D. P., & Davis, M. 1998, ApJ, 500, 525
Srianand, R. 2000, ApJ, 528, 617
Wilson, A. S., Wu, X., Heckman, T. M., Baldwin, J. A., & Balick, B. 1989, ApJ, 339, 729